

# In-situ monitoring and reliability analysis of an embankment slope with soil variability

Tao Bai<sup>1</sup>, Han Yang<sup>1,2</sup>, Xiaobing Chen<sup>\*3</sup>, Shoucheng Zhang<sup>4</sup> and Yuanshang Jin<sup>5</sup>

<sup>1</sup>School of Civil Engineering and Architecture, Wuhan Institute of Technology, Wuhan, China

<sup>2</sup>Wuhan Hengtong Highway Survey and Design Co., Ltd, Wuhan, China

<sup>3</sup>School of Transportation, Southeast University, China

<sup>4</sup>Wuhan Municipal Engineering Design & Research Institute Co., Ltd., Wuhan 430072, China

<sup>5</sup>Liaoning Zhixin Highway Engineering Technology Consulting Corporation, Shenyang, 110000, China

(Received July 8, 2020, Revised October 17, 2020, Accepted October 25, 2020)

**Abstract.** This paper presents an efficient method utilizing user-defined computer functional codes to determine the reliability of an embankment slope with spatially varying soil properties in real time. The soils' mechanical properties varied with the soil layers that had different degrees of compaction and moisture content levels. The Latin Hypercube Sampling (LHS) for the degree of compaction and Kriging simulation of moisture content variation were adopted and programmed to predict their spatial distributions, respectively, that were subsequently used to characterize the spatial distribution of the soil shear strengths. The shear strength parameters were then integrated into the Geostudio command file to determine the safety factor of the embankment slope. An explicit metamodal for the performance function, using the Kriging method, was established and coded to efficiently compute the failure probability of slope with varying moisture contents. Sensitivity analysis showed that the proposed method significantly reduced the computational time compared to Monte Carlo simulation. About 300 times LHS Geostudio computations were needed to optimize precision and efficiency in determining the failure probability. The results also revealed that an embankment slope is prone to high failure risk if the degree of compaction is low and the moisture content is high.

**Keywords:** soil; embankment; compaction; moisture content; slope stability; reliability

## 1. Introduction

The inherent spatial variability (Phoon and Kulhawy 1999, Cho 2012, Chenari *et al.* 2019, Zhao *et al.* 2020) of soil properties has become a research focus for many geotechnical engineers in recent decades, particularly with respect to slope stability and reliability analysis (Saseendran and Dodagoudar 2020). To handle with this problem, the Gauss random field theory was proposed and has been widely used to statistically simulate the actual soil strength distribution and slope stability analysis (Kim *et al.* 2020). The Gauss random field theory successfully provides the possibility of evaluating the slope failure under the influence of inhomogeneous soil properties. However, the key parameter used in this theory is "relative distance" rather than "absolute location" when describing the spatial correlation between the soil samples at different locations within an embankment.

For instance, the existing Gauss random field theory assumes that the soil properties at the bottom of the upper compacted layer are the same or close to the soils at the top distance even though they are located in two different layers of the lower layer as they have a small relative vertical with distinctive degree of compaction. It implies that the effects

of a layered structure in the embankment on the soil properties are not taken into consideration, which does not represent the realistic compaction conditions in the embankment (Liu *et al.* 2017a). In addition, the moisture content, which fundamentally affects the soil strength, is not considered in the slope stability assessment when the relative distance is employed in the Gauss random field theory.

The embankment slope, which is an artificial structure formation, is usually constructed using disturbed soils obtained nearby, transported, and compacted at a given project location. The soil is typically roller compacted into various layers with the optimal soil moisture content maintained to ensure the greatest degree of compaction (i.e., percentage ratio of the measured density to the maximum dry density) of the soil layers. The slope stability is predominantly influenced by the soil shear strength, which in turn directly depends on the degree of compaction and the moisture content of the soil in the embankment.

The degree of compaction for each layer primarily determines the shear strength of the slope soils, which keeps the slope stable when exposed to wheel loads and moisture fluctuations. It is noted that the embankment layers undergo further compaction after construction due to traffic loading, densification, and gravitational settlement (Modoni *et al.* 2018). In practice, however, this additional compaction is often neglected. Theoretically, this is because this additional compaction is beneficial to slope stability and therefore,

---

\*Corresponding author, Associate Professor, Ph.D.  
E-mail: [xbchen@seu.edu.cn](mailto:xbchen@seu.edu.cn)

conservative to design without its consideration. Besides, the soil moisture content fluctuates with time, among others, due to rainy-water infiltration, water evaporation, groundwater level variations, etc. (Liu *et al.* 2017b). On this basis, it can be assumed that the soil shear strength in a constructed embankment slope varies mainly as a function of the soil moisture content.

Some probabilistic analysis methods have been utilized to incorporate geotechnical uncertainties in reliability evaluation to predict the slope safety margin using the failure probability ( $P_f$ ) concept or reliability index ( $\beta$ ). Two of the common probabilistic analysis methods include the first order reliability method (Ji *et al.* 2018) and Monte Carlo (MC) method (El-Ramly *et al.* 2002). Many profound achievements have been made in understanding and utilizing probability-based analysis methods. However, some challenges still exist in the design practice of embankment slopes. These challenges include the difficulties in realizing the random field and calculating the safety factor ( $F_s$ ) for slopes with geotechnical-related uncertainties (El-Ramly *et al.* 2002) and the high computational cost associated with reliability analysis. The other challenge is the implicit relationship between the safety factor and independent variables that often causes confusion with respect to the physical meaning (Hassan and Wolff 1992) of  $\beta$  as it is used to determine the reliability of slopes with floating sliding surfaces or uncertain  $F_s$  expression.

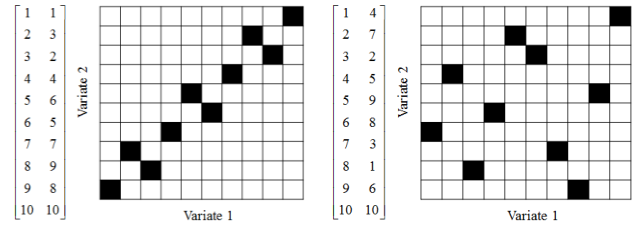
To mitigate these challenges, this study proposes a probability analysis method to efficiently evaluate the slope safety. The in-situ soil moisture content and degree of compaction were firstly measured, and then the strength parameters of slope soil were arbitrarily derived in real time based on the laboratory shear strength tests. The method consists of three components, namely: (a) in-situ layered random field to model the spatial variability of embankment soil properties, (b) secondary development based on *Geostudio 2007* to calculate the safety factor, and, (c) Kriging metamodal for slope reliability assessment. The following sections explain the methods in detail.

## 2. Study methods

The Latin Hypercube Sampling (LHS) and the Kriging methods are the two key methods used in the specimen sampling process and reliability analysis of embankment slopes (McKay *et al.* 1979, Echard *et al.* 2011). These two methods are discussed in the following subsections.

### 2.1 Latin hypercube sampling

Compared to the Monte Carlo (MC) method that samples the specimens randomly in the distribution domain, LHS is a more effective in that it reduces the number of samplings for computational optimization (McKay *et al.* 1979). In order to have an even sampling, the  $i^{\text{th}}$  ( $i=1,2,\dots,M$ ) subspace of  $M$ -dimensional hypercube  $V$  is typically divided into  $N$  disjointed subsets with equal probability. For simplicity, the samples are then back-calculated from the respective strata according to Eq. (1),



(a) Implied correlation (b) Sampling after correlation reduction

Fig. 1 Correlation reduction strategy in sampling action

$$x_{ki} = F^{-1}((k - 0.5)/N); k = 1, 2, \dots, N; i = 1, 2, \dots, M \quad (1)$$

where  $F^{-1}$  is the inverse of cumulative probability density function for each vector component.

Even though the marginal distribution of each variable is discretely taken into consideration, there is a risk that a spurious correlation exists between the samples due to the random pairing of all the vector component samples. Each variable can be sampled discretely in its own subspace using the LHS method. However, the combination of the two variables could be highly correlated as presented in Fig. 1(a). To address this issue, an improved LHS algorithm (Huntington and Lyrintzis 1998, Cioppa and Lucas 2007) with a correlation-reduction procedure was adopted in this study to sample the optimal pairings – see Fig. 1(b) (Olsson and Sandberg 2002).

### 2.2 Kriging metamodal

An explicit result can be obtained if an analytical function is provided. However, most functions are implicit with the need for iterative numerical calculations to achieve explicit results. Additionally, numerous samples and multiple sampling points must be used to ensure computational precision, which is a very time-consuming process. Therefore, a metamodal is proposed to provide an explicit and optimal relationship fitting the original implicit function with limited experimental samplings (i.e., realizations). Then, the validated metamodal such as the Kriging method can be used to optimally process huge realizations that are sampled from a given distribution with high computational efficiency.

#### 2.2.1 Kriging method

The Kriging method was firstly developed for geostatistics in the 1950s by Krige and then improved by Matheron (Echard *et al.* 2011). The Kriging method is typically used to provide a hypercube space curve fitted with limited samples. Then, the function variables can be efficiently determined at any designed sampling points numerically.

For a given sampling set of  $\mathbf{S} = [\mathbf{x}_1, \mathbf{x}_2, \dots, \mathbf{x}_i, \dots, \mathbf{x}_m]$  with  $s_i \in \Omega^m$  and responses  $\mathbf{Y} = [y_1, y_2, \dots, y_i, \dots, y_m]$  with  $y_i \in \Omega^q$ , the deterministic response  $y(x)$  can be expressed as a realization of a regression model  $f(x)^T \boldsymbol{\beta}$  and a random stochastic process  $z(x)$ , expressed in Eq. (2),

$$y(\mathbf{x}) = f(\mathbf{x})^T \boldsymbol{\beta} + z(\mathbf{x}) = \sum_{i=1}^p \beta_i f_i(\mathbf{x}) + z(\mathbf{x}) \quad (2)$$

where,  $f_i(\mathbf{x})$  is a linear combination of  $p$  chosen functions,  $\boldsymbol{\beta} = [\beta_1, \beta_2, \dots, \beta_i, \dots, \beta_p]^T$  are regression parameters,  $z(\mathbf{X})$  is a stationary Gaussian process with zero mean and covariance between two points of space  $\mathbf{X}$  and  $\mathbf{W}$ , which is defined by Eq. (3),

$$\text{cov}(z(\mathbf{X}), z(\mathbf{W})) = \sigma^2 R(\boldsymbol{\theta}, \mathbf{X}, \mathbf{W}) \quad (3)$$

where,  $R(\boldsymbol{\theta}, \mathbf{X}, \mathbf{W})$  is the correlation model with parameters  $\boldsymbol{\theta} = [\theta_1, \theta_2, \dots, \theta_i, \dots, \theta_n]^T$ . In this study, the anisotropic Gaussian model was expressed in Eq. (4)

$$R(\boldsymbol{\theta}, \mathbf{X}, \mathbf{W}) = \exp\left(-\sum_{k=1}^n \theta_k |w_k - x_k|^2\right) \quad (4)$$

where,  $w_k$  and  $x_k$  are the  $k^{\text{th}}$  coordinates of the points  $\mathbf{W}$  and  $\mathbf{X}$ .

The best linear unbiased predictor is then applied to estimate the function value  $\hat{y}(\mathbf{x}_{new})$  for any new point  $\mathbf{x}_{new}$  as shown in Eq. (5),

$$\hat{y}(\mathbf{x}_{new}) = f(\mathbf{x}_{new})^T \hat{\boldsymbol{\beta}} + \mathbf{r}(\mathbf{x}_{new}) \mathbf{R}^{-1} (\mathbf{Y} - \mathbf{F} \hat{\boldsymbol{\beta}}) \quad (5)$$

$$\mathbf{r}(\mathbf{x}_{new}) = \begin{bmatrix} R(\boldsymbol{\theta}, \mathbf{x}_{new}, \mathbf{x}_1) \\ R(\boldsymbol{\theta}, \mathbf{x}_{new}, \mathbf{x}_2) \\ \dots \\ R(\boldsymbol{\theta}, \mathbf{x}_{new}, \mathbf{x}_m) \end{bmatrix}^{-T} \quad (6)$$

$$\mathbf{F} = [f(\mathbf{x}_1), f(\mathbf{x}_2), \dots, f(\mathbf{x}_m)]^T \quad (7)$$

The scalars  $\hat{\boldsymbol{\beta}}$  and variance  $\hat{\sigma}_z^2$  can be evaluated using Eq. (8) and Eq. (9) (Jones *et al.* 1998) provided that  $\boldsymbol{\theta}$  is firstly calculated using the maximum likelihood estimation in Eq. (10).

$$\hat{\boldsymbol{\beta}} = (\mathbf{F}^T \mathbf{R}^{-1} \mathbf{F})^{-1} \mathbf{F}^T \mathbf{R}^{-1} \mathbf{Y} \quad (8)$$

$$\hat{\sigma}_z^2 = \frac{1}{m} (\mathbf{Y} - \mathbf{F} \hat{\boldsymbol{\beta}})^T \mathbf{R}^{-1} (\mathbf{Y} - \mathbf{F} \hat{\boldsymbol{\beta}}) \quad (9)$$

$$\text{Min. } \phi(\boldsymbol{\theta}) = |R(\boldsymbol{\theta}, S)|^{\frac{1}{m}} \hat{\sigma}_z^2 \quad (10)$$

where  $|R|$  is the determinant of  $R$ .

The universal Matlab DACE tool was used in this study to establish the Kriging metamodal as well as the slope performance function discussed below.

### 2.2.2 Performance functional metamodal

In slope engineering, the performance function is usually defined using the expression in Eq. (11).

$$Z = F_s - 1 \quad (11)$$

For an embankment slope with stratigraphic uncertainties at the layer boundaries, the analytical calculation of  $F_s$  is implicit and iteratively solvable through numerical simulations. Accordingly, the performance functional metamodal is also inherently an implicit function.

Simulations of complex structures are always time-consuming, especially for those with multiple inputs and uncertainties. For this reason, the Kriging metamodal was introduced to explicitly approximate  $F_s$  instead of using the original implicit function in Eq. (11), where the Kriging metamodal can greatly improve the computational efficiency and accuracy of the reliability analysis.

In the Kriging metamodal, the shear strength parameters for the  $i^{\text{th}}$  soil layer, such as the cohesion  $c_i$ , friction angle  $\phi_i$ , and gravity  $\gamma_i$ , are ranked sequentially in the vector  $\mathbf{x} = [x_1, x_2, \dots, x_i, \dots, x_n]^T$ . Then, the function values  $\mathbf{Z} = [Z^{(1)}, Z^{(2)}, \dots, Z^{(m)}]^T$  at  $m$  project sites  $\mathbf{S} = [x^{(1)}, x^{(2)}, \dots, x^{(m)}]^T$  can be expressed as Eq. (12), where  $f(\mathbf{x})$  is a zero-order function equal to 1 (Lophaven and Søndergaard 2002).

$$\hat{Z} = \bar{g}(\mathbf{x}_{new}) = \hat{\boldsymbol{\beta}} + \mathbf{r}(\mathbf{x}_{new}) \mathbf{R}^{-1} (\mathbf{Y} - \mathbf{I} \hat{\boldsymbol{\beta}}) \quad (12)$$

## 3. Safety factor computation

An embankment slope with a height of  $h=6$  m and an inclination of 1:1.5 representing a second-class highway in Hubei Province (China) was utilized for demonstrative analysis. As shown in Fig. 2(a), the width is 13 m for the top surface of the right half of the subgrade embankment. In the figure, K96 represents the zone with a degree of compaction of 96% and a depth of 0.8 m from the top surface of subgrade. K94 is the zone, having 94% degree of compaction with a depth ranging from 0.8 m to 1.5 m. K93 is a zone with 93% degree of compaction and a depth range of 1.5 m to 6 m. The layer beneath the original ground was designated as zone K90 zone with a degree of compaction of 90%.

### 3.1 In-situ moisture content

The humidity measuring circuits, namely a *humidity transducer HIH 3610* and *one-wire bus apparatus DS 2438*, were installed to measure moisture contents at 25 different points (A<sub>1</sub>, A<sub>2</sub>, ... E<sub>5</sub>) in the slope section – see Fig. 2(a). These circuits were installed from the bottom layer to the upper layers following the standard Chinese construction procedures of the embankment. The in-situ moisture contents at these selected points were measured in real time, which served as the raw data for the Kriging prediction of the humidity field in the whole slope section.

In addition, field investigation (Deng and Tang 1994) demonstrates that the degree of compaction follows a specific statistical distribution such as normal distribution, lognormal distribution, or extreme value distribution. By neglecting the soil settlement after construction, the spatial

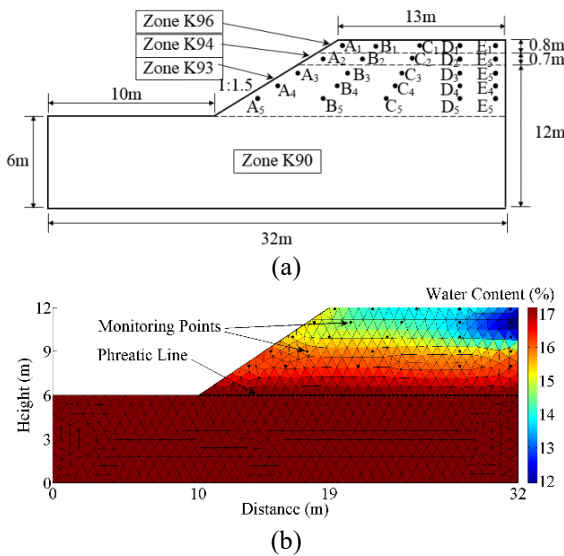


Fig. 2 (a) Embankment slope geometry and (b) Kriging field moisture modeling simulation

variable random field of degree of compaction can be generated based on the probability distribution of multi-layer compacted soils resulting from a field investigation. Then, the random field of shear strength can be determined using numerical calculation by associating the spatial variable random field of degree of compaction with the real-time random field of moisture content (Fig. 2(b)) at a given time. For simplicity, the underground water table was set as the same elevation as the original ground surface.

### 3.2 Degree of compaction distribution

During embankment construction, the original soil is typically distributed and compacted to a designed degree to provide the soil with the desired deformation resistance against traffic loading and gravitational settlement. Using the laboratory determined maximum dry unit weight  $\rho_{\max}$  of the in-situ soil, the degree of compaction  $K$  is defined by Eq. (13) as follows.

$$K = \frac{\rho_d}{\rho_{\max}} \times 100\% \quad (13)$$

where,  $\rho_d$  is the dry unit weight of the in-situ compacted soil and  $\rho_{\max}$  is the soil maximum dry unit weight.

Traffic-load induced stresses generally decrease with soil depth in an embankment. Thus, an embankment is usually subdivided into different layers with different degrees of compaction that decreases with from the top to the lower layers. As presented in Fig. 2(a), zone K96 implies that the representative value of layer degree of compaction is larger than 96%. The same holds for zone K94 and zone K93, i.e., 94% and 96%, respectively.

The in-situ degrees of compaction for zones K93, K94, and K96 were tested to statistically identify their probability distributions. Based on the trial tests with normal, lognormal, and extreme value distribution, the lognormal distribution was selected for optimal modeling of the probability distribution of the degree of layer compaction.

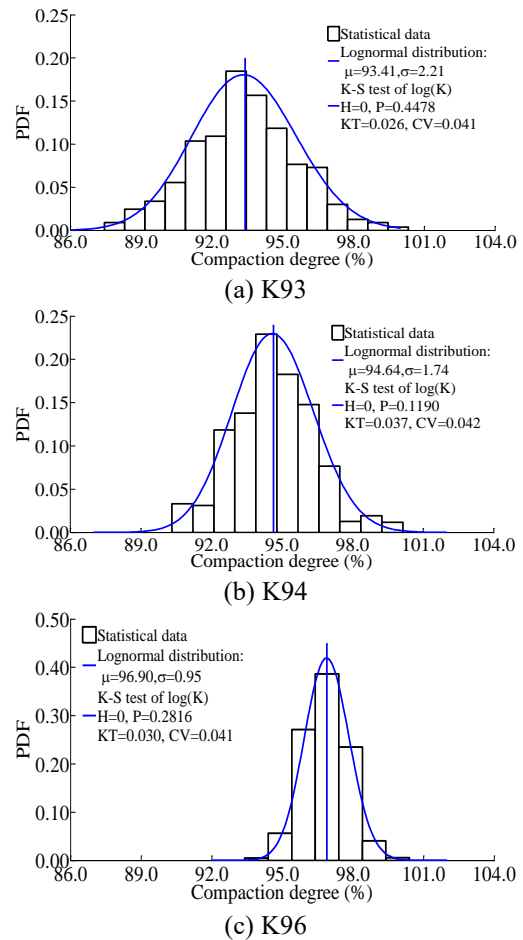


Fig. 3 Probability density function for compaction zones with different degrees of compaction

Logarithmic Kolmogorov-Smirnov (K-S) tests for degree of compaction were then conducted to examine their goodness of fit.

The probability density functions for the three compaction zones (K93, K94, and K96) are shown in Fig. 3. In Fig. 3, KT and CV are the two determining indices for assumption verification. KT is a calculated statistic value of K-S test, while CV means the critical statistic value of the test data. 'H=0' means the original hypothesis could be accepted, simultaneously the KT should be smaller than CV. While 'H=1' means the original hypothesis must be denied. 'P' means the acceptance probability of the original hypothesis.

As evident in the Fig. 3, the hypothesis test passed since  $KT < CV$  for all the three degrees of compaction. Thus, the lognormal distribution was selected to model the degree of compaction distribution and provide the sampling inputs for prediction and estimation of the safety factors. In addition, the 5% significance level was set in the hypothesis testing.

### 3.3 Laboratory shear strength testing

#### 3.3.1 Particle size analysis

A screening sieve test was used to determine the particle composition of the in-situ soil. The sieve analysis and percentage passing results are plotted in Fig. 4. The non-

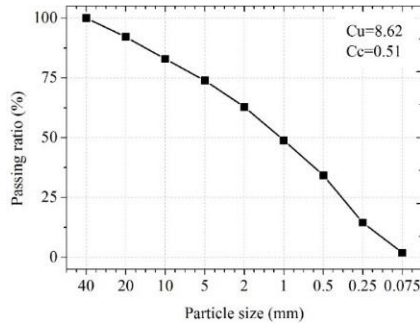


Fig. 4 Gradation of the in-situ soil

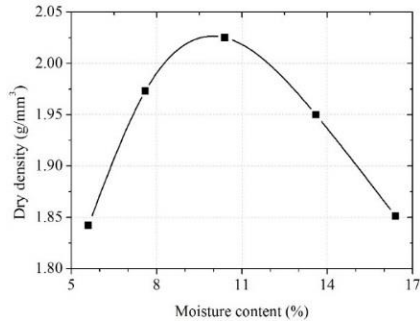


Fig. 5 Relationship between dry unit weight and moisture content

uniformity coefficient  $C_u$  and curvature coefficient  $C_c$  were used to quantify the soil gradation using Eq. (14) and Eq. (15).

$$C_u = \frac{d_{60}}{d_{10}} \quad (14)$$

where,  $d_{60}$ ,  $d_{30}$  and  $d_{10}$  are the diameters of the sieve size through which the soil passing ratio is 60%, 30%, and 10%, respectively.

Soils used in embankment filling requires a  $C_u$  larger than 5 and  $C_c$  from 1 to 3, respectively. In this study, the  $C_u$  and  $C_c$  values are 8.62 and 0.51, respectively, which implies that the in-situ soil is practically not suitable for filling the embankment.

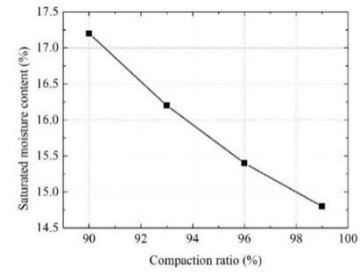
### 3.3.2 Saturated moisture content for soils with different degrees of compaction

Soil is a three-phase material composed of solid particles, water, and air. The saturated water content  $\omega_s$ , is the moisture content at which the internal air voids in the soil structure is fully filled by water. The embankment soil layers with different degrees of compaction possess different air voids. Therefore, their saturated water contents are different from each other. The saturated water contents at different degrees of compaction can be obtained using the following two steps.

**Step 1:** Measurement of the optimum moisture content  $\omega_o$  and the maximum dry unit weight  $\rho_{max}$ . In engineering practice, the embankment layer is constructed and compacted to a designed degree of compaction at its optimum moisture content  $\omega_o$ , which corresponds to the maximum dry unit weight  $\rho_{max}$  in the compaction curve shown in Fig. 5. The curve is obtained from a standard



(a)



(b)

Fig. 6 (a) Soil samples fixed in cascade saturators and (b) Relationship between compaction and saturated moisture content

compaction test (Li *et al.* 2017), which describes the relationship between the dry unit weight of the soil and its moisture content. In this study, the  $\omega_o$  and  $\rho_{max}$  parameters were 10.1% and 2.026 g/cm<sup>3</sup>, respectively.

**Step 2:** Relationship between the degree of compaction and saturated moisture content. The soil samples were firstly moulded in a cutting ring knife at the aforementioned optimum moisture content and degrees of compaction ranging from 90% to 99% with an incremental interval of 3%. At each degree of compaction, five samples were fabricated and fixed in the cascade saturator (Fig. 6(a)).

After being submerged in water for 72 hours, the samples became saturated. Then, all the samples were dried in the oven. The weights for both the saturated and dried samples were measured to compute the saturated water content  $\omega_s$  by Eq. (16).

$$\omega_s = \frac{m_2 - m_3}{m_3 - m_1} \times 100\% \quad (16)$$

where,  $m_1$  is the mass of cutting ring knife;  $m_2$  is the mass summation of a cutting ring knife and the saturated soil sample; and  $m_3$  is the mass summation of a cutting ring knife and the dry soil sample.

Fig. 6(b) presented the relationship between compaction and the saturated moisture content. It is obvious that the saturated moisture content decreases with an increase in the degree of compaction.

### 3.3.3 Direct shear test

In order to investigate the relationship of the soil shear strength with compaction and moisture content, direct shear tests were conducted at different normal pressures. Firstly, the in-situ soil was grounded in the laboratory after drying to constant weight. Then, the soil with particle size less than 2 millimeter was collected by screening the crushed sample. Water with a specified weight of  $m_w$  (6%, 8%, 10.1%, 12% and 14%) was added onto the dried soil samples and kept

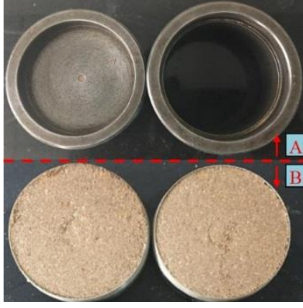


Fig. 7 Sample steel mould and cutting ring knife

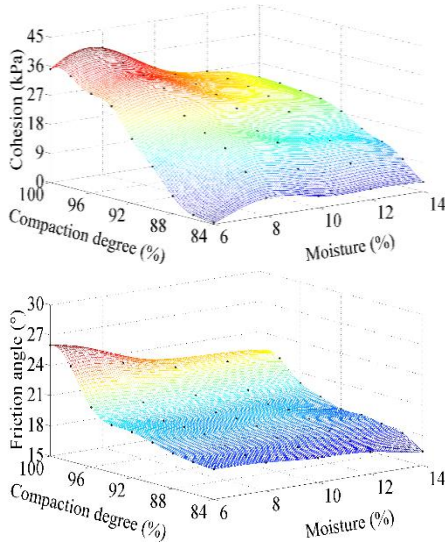


Fig. 8 Kriging model simulation of the shear strength parameters

sealed in a plastic film to ensure homogeneous diffusion of moisture in the soil.

The weight of the wet soil  $m_{so}$  was determined using Eq. (17) and Eq. (18).

$$m_{so} = \rho_d V (1 + 0.01 \times \omega_{ss}) \quad (17)$$

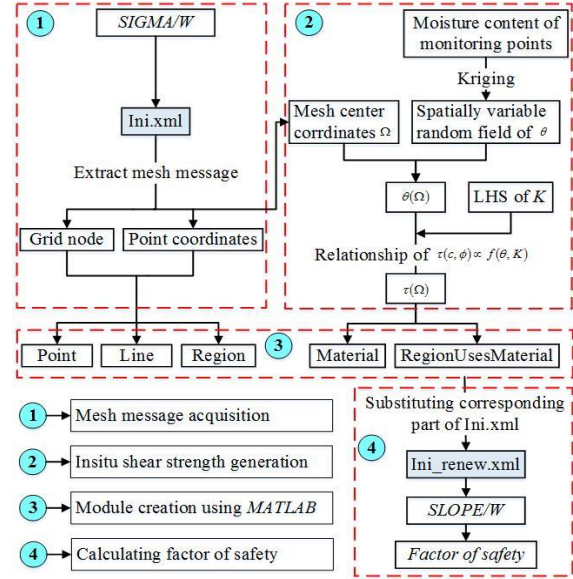
$$\rho_d = K \times \rho_{max} \quad (18)$$

where,  $K$  is the degree of compaction, 84%~98% were used at an incremental rate of 2%;  $\rho_{max}$  is the maximum dry unit weight;  $\omega_{ss}$  is the designed moisture content (%); and  $V$  is the volume of the wet soil samples.

As presented in Fig. 7, the wet soil was transferred into the steel mould (Fig. 7(A)) that was matched with the cutting ring knife (Fig. 7(B)). The soil was pressed directly to the designed degree of compaction in the cutting ring knife with a cylinder diameter of 61.8 mm and height of 20 mm, respectively.

The direct shear test apparatus and the Mohr Coulomb theory were employed to characterize the undrained shear strength properties of the compacted soil. The shear strength parameters, namely the cohesion ( $c$ ) and friction angle ( $\phi$ ), were determined using Eq. (19).

$$\tau = c + \sigma \tan \phi \quad (19)$$

Fig. 9 Safety factor computational flowchart in *Geoslope 2007*

A set of discrete shear strength parameters were obtained and then, the Kriging method was employed to simulate the shear strength parameters over a range of  $K$  (84-100%) and (6-14%) values shown in Fig. 8. Thus, using Fig. 8, the soil shear strength parameters (cohesion and friction angle) can be estimated for a given degree of soil compaction and moisture content. For a given slope, the moisture content functionally varies with time. Consequently, this allowed for the degree of compaction to be the major factor governing the probabilistic analysis of the embankment slope at a given specific time. Ultimately, this permitted for using the LHS method to quantify the degree of compaction.

### 3.4 Calculation of the safety factor

The module *Geoslope 2007* in commercial software *Geostudio 2007* was used to calculate the safety factor ( $F_s$ ) for a slope with spatially variable soil properties. The embankment slope comprised of a compacted multi-layered structure with different degrees of compaction between the layers. The moisture content was considered to vary as a function of location, both vertically and horizontally. For  $F_s$  calculation, the key issue is to establish a valid command script in *Geoslope 2007* to represent the strength variability of the soil slope. Fig. 9 illustrates a 4-step flowchart adapted in this study to determine  $F_s$ , namely:

**Step 1:** Mesh formulation. *Geoslope 2007* cannot be used to directly generate the slope section grid for calculating  $F_s$  as was previously shown in Fig. 2(b). So, *SIGMA/W 2007*, a different module in *Geostudio 2007*, was introduced to formulate the mesh geometry including the grid nodes and point coordinates in a file named *Ini.xml*.

**Step 2:** In-situ shear strength characterization. Based on the LHS of  $K$  and Kriging simulation of  $\theta$ , the shear strength can be determined for the soil slope at any spatial location with different  $K$  and  $\theta$  values in the embankment.

**Step 3:** Module creation using Matlab. The shear strength and the slope geometry were sequentially

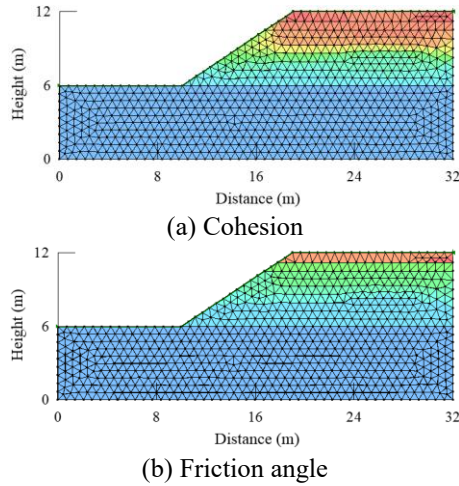


Fig. 10 Graphical illustration of the spatially variable shear strength parameters in the embankment

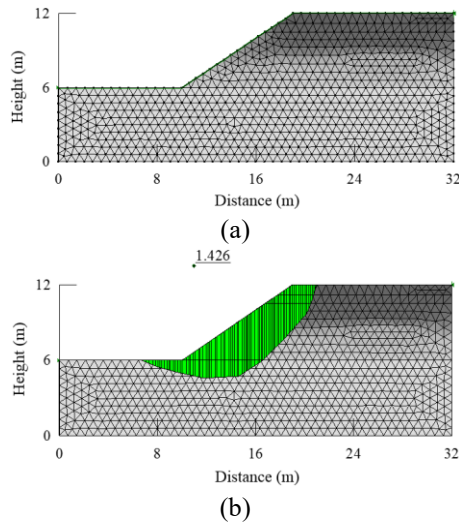


Fig. 11 Diagram of *Ini\_renew.xml* calculated in *Geoslope*: (a) *Ini\_renew.xml* loaded in *Geoslope*; (b)  $F_s$  calculated from *Ini\_renew.xml*

assembled using Matlab. The key point here is that the command format in the module generated using Matlab must be consistent with the original command script *Ini.xml* (Step 1) used in *Geoslope*. In this step, all the modules in *Ini.xml*, such as “Point”, “Line”, “Region”, “Material”, and “RegionUsesMaterial”, are replaced with random characteristics of the soil features.

**Step 4:** Calculation of  $F_s$ . The modules created in Step 3 are used to substitute their counterparts in *Ini.xml*. Then, a new command script, namely file *Ini\_renew.xml*, is used to calculate  $F_s$ .

Fig. 10 shows the spatial distribution of the shear strength parameters including the cohesion and friction angle over the slope section. Both cohesion and friction angle vary along the depth direction, which corresponds to the decreased degree of compaction from the top to lower layers. However, the shear strength varies along the horizontal direction as a function moisture content variation that was previously shown in Fig. 2(b).

Fig. 11 presents the results calculated from

*Ini\_renew.xml* file in *Geoslope*, where the limit equilibrium method (LEM) was used. Note that the slip surface in Fig. 11(b) is a calculation result, rather than a defined sliding face before the calculation. The slip surface was optimized in *Geoslope* as the most crucial unstable sliding face for the embankment slope. As shown in Fig. 11(b), the slip surface is noncircular, but comprises of a range of vertical and individual slices. In Fig. 11(b), the bottom of the individual slice constitutes a segment that is connected to two adjacent intersections between the slip surface and mesh grid.

#### 4. Reliability analysis

Reliability analysis is discussed in this section and includes the following aspects: index selection, analysis procedure, and parametric verification.

##### 4.1 Parametric index selection

The critical boundary condition between a safe region and a failure region for the soil slope occurs when  $Z=0$  in Eq. (11). The failure probability is therefore calculated through integration analysis over the failure domain as shown in Eq. (20):

$$P_f = P[g(\mathbf{X}) \leq 0] = \int_{g(\mathbf{X}) \leq 0} f_{\mathbf{X}}(\mathbf{X}) d\mathbf{X} \quad (20)$$

where  $f_{\mathbf{X}}(\mathbf{X})$  represents the joint probability density function.

Assuming that in  $n_t$ -repeated trials, the occurrence number of an event  $A$  is  $n_c$ , then the frequency occurrence of the event  $A$  is  $n_c/n_t$ . According to the law of large numbers (Kouritzin *et al.* 2016), if the probability of an event  $A$  is  $P(A)$ , then there exists the Eq. (21) for any  $\varepsilon > 0$ :

$$\lim_{n \rightarrow \infty} P\left(\left|\frac{n_c}{n_t} - P(A)\right| < \varepsilon\right) = 1 \quad (21)$$

Eq. (21) means that if the total trial numbers are large enough, then the frequency occurrence of event  $A$  will converge to  $P(A)$  with a probability of 1.0. In this study, the computational extent of reliability analysis was composed of  $m$  times *Geoslope* calculations and  $n$  times Kriging simulations. The parameter  $m$  is the key value affecting the sampling efficiency of the degree of compaction on the whole sampling space, which subsequently greatly influences the precision of failure probability determined by the  $n$  times Kriging simulations.

The failure probability  $P_f$  and reliability index  $\beta$  are the two common indices used in slope reliability analysis. For a standard normal distribution, there is a specific corresponding relationship between  $P_f$  and  $\beta$ . The reliability index is typically obtained from a probability analysis on a chosen slip surface (Hassan and Wolff 1992). However, it should be pointed out that safety factor will become meaningless if it is calculated from trial floating slip surfaces. In this study, for the target was a critical slip surface in the embankment with spatially variable soil properties such as shear strength, moisture content, etc.

In addition, the literature (Su and Yang 2012) indicates that the reliability index can be obtained if the Kriging

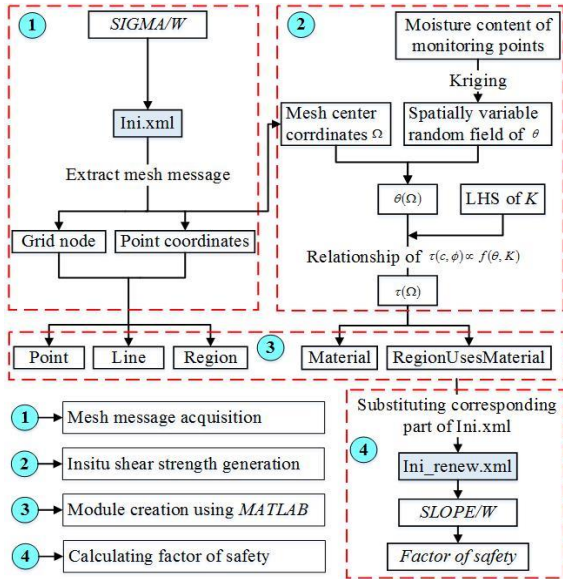


Fig. 12 Flowchart of failure probability analysis

metamodal is established first. However, computational convergence in finding the numerical solutions become a challenge due to that the partial derivative of the reliability index  $\beta$ , which is iteratively calculated as denominator in the analysis model. Thus, the reliability index becomes difficult to obtain when its function is discontinuous in the solution region. Therefore, only the failure probability  $P_f$  was employed in this study to evaluate the slope reliability.

#### 4.2 Reliability analysis procedure

Fig. 12 presents a 3-step flowchart for reliability analysis of an embankment slope taking into account the spatial distribution of the degree of compaction and moisture content.

**Step 1:** In-situ test and numerical simulation of field data to determine the spatial distribution of the soil moisture  $\theta$  and degree of compaction  $K$ . The in-situ moisture contents at the monitoring points were first collected and then, the Kriging method was applied to simulate the spatial distribution of the moisture field. Based on the investigated distribution of the degree of compaction, the LHS method was utilized to model the  $m$  designed sites at a specific degree of compaction  $K$  where  $m$  is the number of sampling points (i.e., realization).

**Step 2:** Laboratory testing to determine the relationship between shear strength and the composition of  $\theta$  and  $K$  parameters. The direct shear tests were conducted on the in-situ soil samples. Then, the obtained relationship of  $\tau(c, \phi) \propto f(\theta, K)$  were used to compute the shear strength of any point in the embankment slope section with different  $\theta$  and  $K$  values.

**Step 3:** Calculation of safety factor and failure probability. At a given monitoring time, the spatial distribution of the in-situ moisture content in the embankment slope section remains unchanged, which can be simulated by the aforementioned Kriging method. Thus, for a given embankment slope at the giving monitoring

Table 1 Failure probability calculations for 2017/07/11

Group	$F_s$ calculation method	Sampling method (realizations)	$P(\%)$	Computation time (s)
A	Morgenstern-Price	Monte Carlo (100000)	27.7	$3 \times 10^6$
B	Morgenstern-Price	LHS (600) +Kriging (100000)	27.0	$1.8 \times 10^4$
C	Bishop	Monte Carlo (100000)	9.1	$3 \times 10^6$
D	Bishop	LHS (600) +Kriging (100000)	10.7	$1.8 \times 10^4$
E	Janbu	Monte Carlo (100000)	2.5	$3 \times 10^6$
F	Janbu	LHS (600) +Kriging (100000)	3.6	$1.8 \times 10^4$
G	Ordinary	Monte Carlo (100000)	15.5	$3 \times 10^6$
H	Ordinary	LHS (600) +Kriging (100000)	17.2	$1.8 \times 10^4$

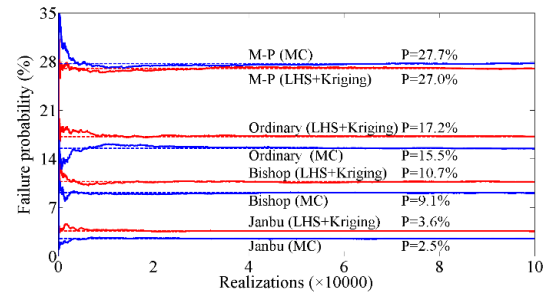


Fig. 13 Failure probability analyses using different LEMs and sampling methods

time, the degree of compaction becomes the only factor affecting the shear strength and the factor of safety. The  $m$  designed sites for the degree of compaction  $K$  in Step 1 contributes to the  $m$  original *.xml* files for computations in the commercial software *Geoslope 2007*.

On the basis of it, the  $m$  safety factors can be determined and used to construct the metamodal performance function. Then, the MC method is introduced for  $n$  times bulk sampling of the degree of compaction  $K$ , where the corresponding safety factors could be calculated for each composition of  $K$  value.

The highlight hereby lies in that the Kriging metamodal can significantly reduce the huge computational time, which is caused by the MC method for the  $F_s$  calculations using *Geoslope 2007*. By contrast, the metamodal is established using only  $m$  times of *Geoslope* calculations. Then, the  $F_s$  for all the sampling points are based on mathematical interpolation, which saves the computational time greatly. For example, the MC method takes about 30 seconds to obtain the  $F_s$  of a spatially variable slope from the *.xml* file using *Geoslope 2007* and a computer with a CPU frequency of 3.3 GHz and random access memory of 8G Bytes. On the contrary, the calculation time was reduced to  $5 \times 10^{-5}$  seconds using the Kriging metamodal. This also implies that the key issue controlling the efficiency of the reliability analysis lies in the calculation of  $F_s$  for the LHS samples.

In this step, the batch program was used for continuous calculations and automatic prediction of the safety factor. Then, the obtained  $F_s$  values were conveniently adopted for reliability analysis. Otherwise, the  $F_s$  values can only be obtained from the graphical user interface of the *Geoslope*

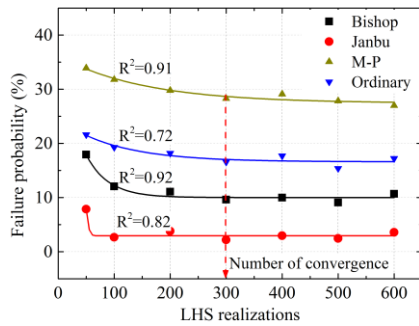


Fig. 14 Influence of LHS realizations on the failure probability

software one by one, which is impossible for this type of analysis.

### 4.3 Parametric verification

The slope failure probability converges as the number of Kriging simulations ( $n$ ) grows. In this study, a total of 19 times in-situ moisture monitoring were performed with the failure probability calculations for the highest moisture content (2017/07/11) exemplified in Table 1.

A trial combination of  $m=600$  and  $n=100000$  was used to evaluate the failure probability of the embankment slope. The Monte Carlo (MC) method was simultaneously used to provide the control solutions for comparison purposes. As can be seen in Table 1 and Fig. 13, the two sampling methods yielded a similar level of failure risk, which implies that the proposed sampling combination of LHS+Kriging method is capable of effectively assessing the slope status. For further comparisons, the Bishop, Janbu, and Ordinary methods were also employed to analyze the slope failure probability for the same conditions, respectively. Fig. 13 shows that there exists some big differences among the methods. The M-P method presents the highest failure probability due to its assumption of mechanical equilibrium conditions (Bai *et al.* 2014, 2018).

In order to further reduce the computational time, the LHS number was set at 50, 100, 200, 300, 400, 500 and 600, respectively, in order to evaluate the effects of the numbers of sampling points on the slope failure probability. However, the computational sampling points for the Kriging simulation ( $n$ ) remained at 100000. Fig. 14 presents the influence of LHS realizations on the final failure probability.

The least square method was used for convergence fitting as the LHS realizations increased. Apparently, the failure probability remained the same for  $m$  equals to or is greater than 300. Thus, the combination of  $m=300$  and  $n=100000$  were adopted for sensitive analysis. This combination potentially cut the computational time by 50% while simultaneously providing the same level of failure probability.

## 5. Sensitivity analysis

The sensitivity analysis is presented and discussed in

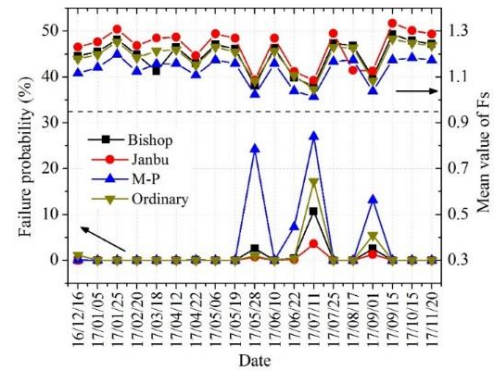


Fig. 15 Graphical plot of the slope failure probability as a function of time

Table 2 Orthogonal test factors for the mean value of the compaction degree

Zone	Variation level (%)		
K96	96.9	95.9	94.9
K94	94.6	93.6	92.6
K93	93.4	92.4	91.4

Table 3  $L_9(3^4)$  orthogonal test design for the mean value of the compaction degree

Compaction degree	K96	K94	K93
1	96.9	94.6	93.4
2	96.9	93.6	92.1
3	96.9	92.6	91.4
4	95.9	94.6	92.4
5	95.9	93.6	91.4
6	95.9	92.6	93.4
7	94.9	94.6	91.4
8	94.9	93.6	93.4
9	94.9	92.6	92.4

Table 4 Orthogonal test results of the mean value of the compaction degree (2017/07/11, high moisture content)

N	Bishop		Janbu		M-P		Ordinary	
	P (%)	Mean of $F_s$	P (%)	Mean of $F_s$	P (%)	Mean of $F_s$	P (%)	Mean of $F_s$
1	8.565	1.06	2.467	1.08	31.042	1.01	16.691	1.05
2	14.428	1.05	6.834	1.07	41.599	1.00	23.155	1.04
3	23.443	1.03	16.875	1.05	64.757	0.99	33.716	1.02
4	12.695	1.05	7.321	1.08	40.572	1.01	21.155	1.03
5	25.096	1.03	16.697	1.06	51.651	0.99	32.532	1.02
6	10.328	1.06	3.316	1.09	32.646	1.02	18.695	1.04
7	23.077	1.04	16.373	1.06	49.537	0.99	32.075	1.02
8	9.182	1.06	2.981	1.09	33.614	1.01	17.138	1.04
9	15.077	1.05	8.132	1.08	41.591	1.00	22.672	1.03

this section. This includes the failure probability time-history curves and degree of compaction analyses.

Table 6 Variation range (R, %) of failure probability (2017/07/11, high moisture content)

	Mean K	Bishop	Janbu	M-P	Ordinary
K96	96.9	15.5	8.7	45.8	24.5
	95.9	16.0	9.1	41.6	24.1
	94.9	15.8	9.2	41.6	24.0
R (%)	/	<b>0.5</b>	<b>0.5</b>	<b>4.2</b>	<b>0.5</b>
K 94	94.6	14.8	8.7	40.4	23.3
	93.6	16.2	8.8	42.3	24.3
	92.6	16.3	9.4	46.3	25.0
R (%)	/	<b>1.5</b>	<b>0.7</b>	<b>5.9</b>	<b>1.7</b>
K93	93.4	9.4	2.9	32.4	17.5
	92.4	14.1	7.4	41.3	22.3
	91.4	23.9	16.6	55.3	32.8
R (%)	/	<b>14.5</b>	<b>13.7</b>	<b>22.9</b>	<b>15.3</b>

5.1 Failure probability time-history curve analysis

For an embankment slope, the degree of compaction is controlled and deemed constant after construction. The slope stability is highly dependent on the inherent moisture content of the soils. Fig. 15 presents the slope stability for a 12 months period from 2016/12/16 to 2017/11/20. Theoretically, Fig. 15 means that the embankment safety can be monitored in real-time if the in-situ moisture is continuously obtained.

As presented in Fig. 15, the mean value of the slope safety factor ( $F_s$ ) and the failure probability are the two main factors governing the slope stability analysis. It is evident that a negative correlation exists between these two factors. Therefore, it is reasonable to adopt these two factors to assess the slope reliability because the failure probability can serve as an early warning of potential slope failure, and it is complementary to the safety factor that is only a deterministic assessment of the slope safety.

5.2 Sensitivity analysis for the degree of compaction

Sensitivity analysis was conducted to assess the influence of construction quality on the operation risk of the embankment. The mean value of the degree of compaction  $\mu_K$  and the standard deviation of degree of compaction  $\sigma_K$  were investigated using orthogonal experimental designs. For comparison purposes, the embankment conditions on the two dates of 2017/07/11 and 2017/09/15 were selected for evaluation. The moisture content of the embankment slope on 2017/07/11 was the highest while it was relatively low on 2017/09/15.

5.2.1 Mean value

For each zone K96, K94, and K93, three different levels of  $\mu_K$  were selected as shown in Table 2. The  $L_9(3^4)$  orthogonal array was used to determine the orthogonal test combinations that are presented in Table 3, where N=9 hereby.

Reliability analysis was carried out for the 9 orthogonal

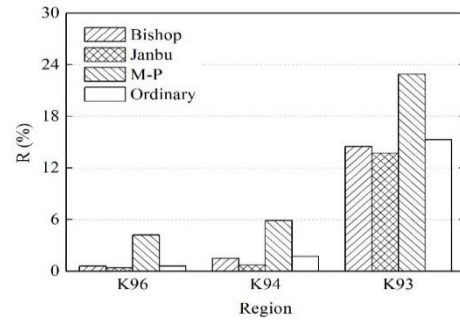


Fig. 16 Variation range of failure probability (2017/07/11, high moisture content)

Table 7 Orthogonal test factors for the standard deviation of the degree of compaction

Zone	Variation level			
K96	1.0	0.7	0.4	0.1
K94	1.7	1.4	1.1	0.8
K93	2.2	1.9	1.6	1.3

Table 8  $L_{16}(4^5)$  orthogonal test design for the standard deviation of the degree of compaction

N	K96	K94	K93
1	1.0	1.7	2.2
2	1.0	1.4	1.9
3	1.0	1.1	1.6
4	1.0	0.8	1.3
5	0.7	1.7	1.9
6	0.7	1.4	2.2
7	0.7	1.1	1.3
8	0.7	0.8	1.6
9	0.4	1.7	1.6
10	0.4	1.4	1.3
11	0.4	1.1	2.2
12	0.4	0.8	1.9
13	0.1	1.7	1.3
14	0.1	1.4	1.6
15	0.1	1.1	1.9
16	0.1	0.8	2.2

tests (Table 3) using the combination of LHS and Kriging methods. The results are shown in Table 4 (2017/07/11 for the high moisture content case) and Table 5 (2017/09/15 for the low moisture content case), respectively.

It is seen in Table 5 that failure may occur for the slope at very low moisture contents. The failure happens when zone K93 has very low degree of compaction as shown in realizations 3, 5, and 7. Therefore, the construction quality should be assured for a stable embankment slope, especially for zone K93. As the moisture content increased, the failure probability increased significantly when comparing Table 5 to Table 4. The range analysis method was adopted to evaluate the influence of layer compaction degree on the

Table 9 Orthogonal test results for the standard deviation of compaction degree (2017/07/11, high moisture content)

N	Bishop		Janbu		M-P		Ordinary	
	P (%)	Mean of Fs	P (%)	Mean of Fs	P (%)	Mean of Fs	P (%)	Mean of Fs
1	8.565	1.06	2.467	1.08	31.042	1.01	16.691	1.05
2	8.490	1.06	1.237	1.08	27.781	1.01	17.351	1.05
3	7.663	1.06	1.196	1.08	21.146	1.01	14.529	1.05
4	5.796	1.06	0.513	1.08	22.236	1.01	15.096	1.05
5	9.582	1.06	1.561	1.08	28.276	1.01	15.979	1.04
6	7.017	1.06	1.640	1.09	30.605	1.02	18.430	1.05
7	4.844	1.06	0.399	1.09	26.034	1.01	13.235	1.05
8	9.679	1.06	2.556	1.08	24.765	1.01	14.584	1.05
9	8.919	1.06	0.935	1.08	28.352	1.01	6.689	1.05
10	5.589	1.06	0.346	1.09	19.319	1.01	13.142	1.05
11	8.464	1.06	1.196	1.09	29.364	1.02	16.286	1.05
12	8.919	1.06	1.288	1.09	27.323	1.02	15.130	1.04
13	4.948	1.06	0.253	1.09	18.403	1.01	12.993	1.05
14	7.337	1.06	0.516	1.09	25.051	1.01	16.464	1.04
15	8.806	1.06	2.071	1.09	23.404	1.02	14.373	1.04
16	10.585	1.07	4.507	1.09	29.261	1.02	15.999	1.04

Table 10 Orthogonal test results for the standard deviation of compaction degree (2017/09/15, low moisture content)

N	Bishop		Janbu		M-P		Ordinary	
	P (%)	Mean of Fs	P (%)	Mean of Fs	P (%)	Mean of Fs	P (%)	Mean of Fs
1	0.000	1.29	0.000	1.34	0.000	1.17	0.000	1.27
2	0.000	1.29	0.000	1.34	0.000	1.17	0.000	1.27
3	0.000	1.29	0.000	1.34	0.000	1.17	0.000	1.17
4	0.000	1.29	0.000	1.34	0.000	1.17	0.000	1.27
5	0.000	1.29	0.000	1.34	0.000	1.17	0.000	1.27
6	0.000	1.29	0.000	1.34	0.000	1.17	0.000	1.27
7	0.000	1.29	0.000	1.35	0.000	1.17	0.000	1.27
8	0.000	1.29	0.000	1.34	0.000	1.17	0.000	1.27
9	0.000	1.29	0.000	1.34	0.000	1.17	0.000	1.27
10	0.000	1.29	0.000	1.34	0.000	1.17	0.000	1.27
11	0.000	1.29	0.000	1.34	0.000	1.17	0.000	1.26
12	0.000	1.29	0.000	1.34	0.000	1.17	0.000	1.27
13	0.000	1.29	0.000	1.34	0.000	1.17	0.000	1.27
14	0.000	1.29	0.000	1.34	0.000	1.17	0.000	1.27
15	0.000	1.29	0.000	1.34	0.000	1.17	0.000	1.27
16	0.000	1.29	0.000	1.34	0.000	1.17	0.000	1.27

slope stability. Table 6 presents the failure probability as calculated from Table 4.

Fig. 16 illustrates the variation ranges of the failure probability for the compaction zones with different degrees of compaction. It is evident that the slope failure is more critical for the low compacted layers such as K93 than the highly compacted layers such as K94 and K96 when the

Table 11 Variation range of failure probability (2017/09/15, low moisture content)

	$\sigma_K$	Bishop	Janbu	M-P	Ordinary
K96 (%)	1.0	7.6	1.4	25.6	15.9
	0.7	7.8	1.5	27.4	15.6
	0.4	8.0	0.9	26.1	12.8
	0.1	7.9	1.8	24.0	15.0
R (%)		<b>0.4</b>	<b>0.9</b>	<b>3.4</b>	<b>3.1</b>
K94 (%)	1.7	8.0	1.3	26.5	13.1
	1.4	7.1	0.9	25.7	16.3
	1.1	7.4	1.2	25.0	14.6
	0.8	8.7	2.2	25.9	15.2
R (%)		<b>1.6</b>	<b>1.3</b>	<b>1.5</b>	<b>3.2</b>
K93 (%)	2.2	8.7	2.5	30.1	16.9
	1.9	8.9	1.5	26.7	15.7
	1.6	8.4	1.3	24.8	13.1
	1.3	5.3	0.4	21.5	13.6
R (%)		<b>3.6</b>	<b>2.1</b>	<b>8.6</b>	<b>3.8</b>

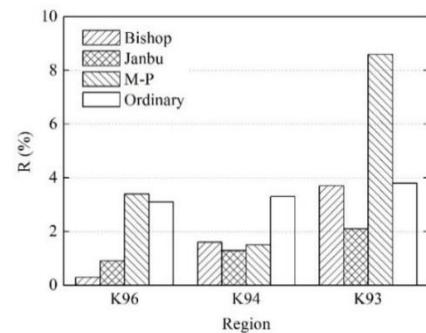


Fig. 17 Variation range of failure probability (2017/09/15, low moisture content)

internal moisture is saturated. The degree of compaction of K93 dominates the slope stability, followed by K94 and then K96. This means that the embankment would collapse rapidly for a slope with a lower degree of compaction and higher water content.

### 5.2.2 Standard deviation

The standard deviation of the degree of compaction  $\sigma_K$  was taken as the variation factor in the orthogonal test for the zones K96, K94, and K93. For each zone, four levels of  $\sigma_K$  are taken as a set as shown in Table 7. The  $L_{16}(4^5)$  orthogonal array was used to specify the orthogonal test combinations, as presented in Table 8, where N=16.

Reliability analysis was carried out for 16 orthogonal group tests using a combination of LHS sampling and Kriging simulations. The results are shown in Table 9 (2017/07/11) for the soils with a high moisture content and Table 10 (2017/09/15) for the soils with a low moisture content, respectively.

It is evident from Table 10 that the slope with low moisture can be safe if  $\sigma_K$  shows small variations. With an increase in the internal moisture content, the failure

probability increases rapidly as shown in Table 9. The range analysis method was adopted to evaluate the influence of the degree of compaction on the slope stability. Table 11 presents the failure probability as calculated using data from Table 9.

Fig. 17 presents the same conclusions as that from Fig. 16, which implies that the slope stability depends more on  $\sigma_K$  of zone K93. In order to enhance the embankment slope safety, engineering methods should be adopted to raise the mean degree of compaction  $\mu_K$  and simultaneously reduce the variation of the compaction  $\sigma_K$ , especially for zone K93 in the embankment.

## 6. Conclusions

This paper presented a method to efficiently evaluate the slope stability within a probabilistic framework based on: (1) the variation of moisture content and degree of compaction of the in-situ embankment soils, (2) user-defined computer codes to determine the spatial distribution of the shear strength parameters of the soil embankment, and (3) the Kriging metamodal method for functional model and performance prediction. The proposed methodology was applied to assess the failure probability of an embankment slope with spatially varying soil properties in real time. From the study results and findings, the following conclusions were drawn:

1. For a given embankment slope, the moisture content was found to be a key factor dominating the slope stability when the statistical distribution of the degree of compaction is deemed unchanged during construction. The spatial distributions of the degree of compaction and moisture content can be used to determine the shear strength parameters and safety factor for the embankment slope stability.

2. The proposed methodology using  $m=300$  times *Geoslope* calculations and  $n=100000$  times Kriging simulations presented comparable predictions of the slope failure probability with those obtained by the Monte Carlo method. However, the proposed methodology reduces the computational time greatly significantly from 30 sec to  $5 \times 10^{-5}$  sec to determine the safety factor for an embankment slope with spatially variable soil properties.

3. The Kriging metamodal of performance function is capable of evaluating the slope stability in real time. The temporal distribution of the slope stability is obtained for the selected slope, which can serve as an early-warning of the slope failure if the in-situ moisture contents is monitored.

4. As theoretically expected, the slope with a low degree of compaction and a high moisture content indicated a high probability failure such as collapsing, differential movement, gravitational settlement, etc. Additionally, the study highlighted the critical need to enhance the mean degree of compaction while simultaneously reducing compaction variability, in particular for lowly compacted embankment sections.

## Acknowledgements

This work was jointly supported by the Science and

Technology Project of Wuhan Municipal Engineering Design & Research Institute Co., Ltd. (grant number H00446), Plan of Outstanding Young and Middle-aged Scientific and Technological Innovation Team in Universities of Hubei Province (grant number T2020010), Natural Science Foundation of Hubei Province (grant number 2020CFB567), and the Science and Technology Project of Ministry of Transport of the People's Republic of China. The authors also greatly appreciate and gratefully acknowledges the sponsors' funding support.

## References

- Bai, T., Hu, X.D. and Gu, F. (2019), "Practice of searching a noncircular critical slip surface in a slope with soil variability", *Int. J. Geomech.*, **19**(3), 04018199 1-13. [https://doi.org/10.1061/\(ASCE\)gm.1943-5622.0001350](https://doi.org/10.1061/(ASCE)gm.1943-5622.0001350).
- Bai, T., Qiu, T., Huang, X.M. and Li, C. (2014), "Locating global critical slip surface using the Morgenstern-Price method and optimization technique", *Int. J. Geomech.*, **4**(2), 319-325. [https://doi.org/10.1061/\(ASCE\)gm.1943-5622.0000312](https://doi.org/10.1061/(ASCE)gm.1943-5622.0000312).
- Chenari, R.J., Fatahi, B., Ghoreishi, M. and Taleb, A. (2019), "Physical and numerical modelling of the inherent variability of shear strength in soil mechanics", *Geomech. Eng.*, **17**(1), 31-45. <https://doi.org/10.12989/gae.2019.17.1.031>.
- Cho, S.E. (2012), "Probabilistic analysis of seepage that considers the spatial variability of permeability for an embankment on soil foundation", *Eng. Geol.*, **133**(3), 30-39. <https://doi.org/10.1016/j.enggeo.2012.02.013>.
- Cioppa, T. and Lucas, T. (2007), "Efficient nearly orthogonal and space-filling Latin hypercubes", *Technometrics*, **49**(1), 45-55. <https://doi.org/10.1198/004017006000000453>.
- Deng, W.D. and Tang, X.Y. (1994), "Statistical analysis of physical parameters of embankment fill", *J. Chongqing Jiaotong Inst.*, **13**(2), 69-76 (in Chinese).
- Echard, B., Gayton, N. and Lemaire, M. (2011), "AK-MCS: An active learning reliability method combining Kriging and Monte Carlo Simulation", *Struct. Saf.*, **33**(2), 145-154. <https://doi.org/10.1016/j.strusafe.2011.01.002>.
- El-Ramly, H., Morgenstern, N.R. and Cruden, D.M. (2002), "Probabilistic slope stability analysis for practice", *Can. Geotech. J.*, **39**(3), 665-683. <https://doi.org/10.1139/t02-034>.
- Hassan, A.M. and Wolff, T.F. (1992), "Search algorithm for minimum reliability index of earth slope", *J. Geotech. Geoenviron. Eng.*, **125**(4), 301-308. [https://doi.org/10.1061/\(ASCE\)1090-0241\(1999\)125:4\(301\)](https://doi.org/10.1061/(ASCE)1090-0241(1999)125:4(301)).
- Huntington, D. and Lyrintzis, C. (1998), "Improvements to and limitations of Latin hypercube sampling", *Probabilist. Eng. Mech.*, **13**(4), 245-253. [https://doi.org/10.1016/S0266-8920\(97\)00013-1](https://doi.org/10.1016/S0266-8920(97)00013-1).
- Ji, J., Zhang, C.S., Gao, Y.F. and Kodikara, J. (2018), "Effect of 2D spatial variability on slope reliability: A simplified FORM analysis", *Geosci. Front.*, **9**(6), 1631-1638. <https://doi.org/10.1016/j.gsf.2017.08.004>.
- Jones, D.R., Schonlau, M. and Welch, W.J. (1998), "Efficient global optimization of expensive black-box functions", *J. Global Optim.*, **13**(4), 455-492. <https://doi.org/10.1023/A:1008306431147>.
- Kim, J.M., Lee, S., Park, J.Y., Kihm, J.H. and Park, S. (2020), "A set of failure variables for analyzing stability of slopes and tunnels", *Geomech. Eng.*, **20**(3), 175-189. <https://doi.org/10.12989/gae.2020.20.3.175>.
- Kouritzin, M.A., Lê, K. and Sezer, D. (2016), "Laws of large numbers for supercritical branching Gaussian processes", *Stoch. Proc. Appl.*, **129**(9), 3463-3498.

- <https://doi.org/10.1016/j.spa.2018.09.011>.
- Li, L., Lin, C. and Zhang, Z.G. (2017), "Utilization of shale-clay mixtures as a landfill liner material to retain heavy metals", *Mater. Design*, **114**, 73-82.  
<https://doi.org/10.1016/j.matdes.2016.10.046>.
- Liu, K., Vardon, P.J., Hicks, M.A. and Arnold, P. (2017b), "Combined effect of hysteresis and heterogeneity on the stability of an embankment under transient seepage", *Eng. Geol.*, **219**(9), 140-150.  
<https://doi.org/10.1016/j.enggeo.2016.11.011>.
- Liu, L.L., Cheng, Y.M., Wang, X.M., Zhang, S.H. and Wu, Z.H. (2017a), "System reliability analysis and risk assessment of a layered slope in spatially variable soils considering stratigraphic boundary uncertainty", *Comput. Geotech.*, **89**, 213-225.  
<https://doi.org/10.1016/j.compgeo.2017.05.014>.
- Lophaven, S. N. and Søndergaard, J. (2002), DACE-A MATLAB Kriging Toolbox Version 2.0, Technical Report IMM-TR-2002-12, 1-25.
- McKay, M.D., Conover, W.J. and Beckman, R.J. (1979), "A comparison of three methods for selecting values of input variables in the analysis of output from a computer code", *Technometrics*, **21**(2), 239-245.  
<https://doi.org/10.1080/00401706.1979.10489755>.
- Modoni, G., Albano, M., Salvatore, E. and Koseki, J. (2018), "Effects of compaction on the seismic performance of embankments built with gravel", *Soil Dyn. Earthq. Eng.*, **106**, 231-242. <https://doi.org/10.1016/j.soildyn.2018.01.005>.
- Olsson, A.M.J. and Sandberg, G.E. (2002), "Latin hypercube sampling for stochastic finite element analysis", *J. Eng. Mech.*, **128**(1), 121-125.  
[https://doi.org/10.1061/\(ASCE\)0733-9399\(2002\)128:1\(121\)](https://doi.org/10.1061/(ASCE)0733-9399(2002)128:1(121)).
- Phoon, K.K. and Kulhawy, F.H. (1999), "Characterization of geotechnical variability", *Can. Geotech. J.*, **36**(4), 612-624.  
<https://doi.org/10.1139/t99-038>.
- Saseendran, R. and Dodagoudar, G.R. (2020), "Reliability analysis of slopes stabilised with piles using response surface method" *Geomech. Eng.*, **21**(6), 513-525.  
<https://doi.org/10.12989/gae.2020.21.6.513>.
- Su, Y.H. and Yang, H.B. (2012), "Reliability algorithm of slope stability based on Kriging metamodel", *Chin. J. Appl. Mech.*, **29**(6), 705-710 (in Chinese).
- Zhao, L.Y., Huang, Y., Xiong, M. and Ye, G.B. (2020), "Reliability and risk assessment for rainfall-induced slope failure in spatially variable soils", *Geomech. Eng.*, **22**(3), 207-217.  
<https://doi.org/10.12989/gae.2020.22.3.207>.